PHYSICAL REVIEW E **77**, 035301(R) (2008)

Herringbone streaks in Taylor-Couette turbulence

S. Dong
Center for Computational & Applied Mathematics, Department of Mathematics, Purdue University, West Lafayette, Indiana 47907, USA

(Received 27 September 2007; revised manuscript received 21 February 2008; published 19 March 2008)

We study near-wall streaks that form herringbonelike patterns in Taylor-Couette turbulence and in counter-rotating Taylor-Couette turbulence through three-dimensional direct numerical simulations. The orientation, axial distribution, onset, and tilting angle of these streaks are characterized.

DOI: 10.1103/PhysRevE.77.035301 PACS number(s): 47.20.Ma, 47.20.Qr, 47.27.−i, 47.32.Ef

Since the earliest studies around a century ago [1,2], Taylor-Couette flow has been the focus of a very large number of experimental and theoretical investigations [3–6]. The majority of the early work has concerned the primary instability, but in the past three decades or so a significant number of studies have examined regimes at high cylinder rotation rates. At high Reynolds numbers the flow accommodates a surprising wealth of states and exhibits remarkable phenomena and pattern formations, e.g., bursting and spiral turbulence [6–10].

One of the most intriguing phenomena of Taylor-Couette turbulence is the formation of near-wall organized patterns with scales much smaller than that of Taylor vortices. Barcilon *et al.* [11] showed photographs (aluminum particle visualization) of numerous fine streaks on the outer cylinder wall in Taylor-Couette flow (inner-wall rotating, outer-wall fixed). The most striking feature of these streaks was that they tilted alternately at small angles with respect to the plane normal to the cylinder axis, forming "herringbonelike" patterns. Figure 1 shows such a pattern, not from experiment, but from numerical simulations reported here. Near-wall streaky regions are a hallmark of turbulence and have been observed in several types of flows, e.g., boundary layers, channel, and plane Couette flow [12,13]. What is unique and remarkable in Taylor-Couette turbulence is the intricate herringbonelike patterns these streaks form and their preferential distribution at certain axial locations of the walls.

Since the revealing of their presence in Taylor-Couette turbulence, only limited insights have been gained about these herringbone streaks. A subsequent theoretical study by Barcilon and Brindley [14] attempted to relate the herringbone patterns to Görtler vortices [15] using a mathematical model. Later, a visualization study [16] reported the observation of Görtler vortices at the inner cylinder wall at Reynolds numbers an order of magnitude lower than that in [11]. So far near-wall herringbone streaks have remained largely a mystery. Much of their characteristics are unknown.

In this Rapid Communication we report the first direct numerical simulation of herringbone streaks in turbulent Taylor-Couette flow and in counter-rotating turbulent Taylor-Couette flow, and characterize several aspects of these streaks. By Taylor-Couette flow we refer to the case with the inner cylinder rotating and the outer one fixed (denoted by TC flow hereafter), and by counter-rotating Taylor-Couette flow we refer to the case with the inner and outer cylinders rotating in opposite directions (denoted by CRTC flow hereafter). The flow geometry is characterized by the radius ratio $\eta=R_i/R_o$ and the aspect ratio $\Gamma=L_z/d$, where L_z, R_i, and R_o are, respectively, the axial dimension and inner and outer radii of the cylinders, and d is the gap width $d=R_o-R_i$. The axis of the concentric cylinders is assumed to coincide with the z axis. The inner cylinder rotates counterclockwise (when viewed toward the $-z$ direction) at a constant angular velocity Ω_i, while the outer cylinder rotates at a constant angular velocity Ω_o ($\Omega_o=0$ for TC flow, $\Omega_o<0$ for CRTC flow). We define the inner- and outer-wall Reynolds numbers as $\mathrm{Re}_i=U_i d/\nu$ and $\mathrm{Re}_o=U_o d/\nu$, where $U_i=\Omega_i R_i$ and $U_o=\Omega_o R_o$ are the inner- and outer-wall velocities, respectively, and ν is the fluid kinematic viscosity. We define "the Reynolds number" as $\mathrm{Re}=\mathrm{Re}_i-\mathrm{Re}_o$ (for TC flow, $\mathrm{Re}=\mathrm{Re}_i$).

Numerically, we solve the three-dimensional incompressible Navier-Stokes equations employing a Fourier spectral expansion of flow variables in the z direction, assuming that the flow is periodic at $z=0$ and $z=L_z$, and a spectral element discretization of the annular domain in x-y planes [17]. A time-marching scheme with a third-order accuracy is employed for temporal integration [18]. No slip boundary conditions are imposed on both cylinder walls. The extensive resolution tests and comparisons with experimental data for validation are documented in [17]. For the TC flow the Reynolds number ranges from $\mathrm{Re}=2000$ to 8000; for the CRTC flow the inner- and outer-wall Reynolds numbers range from 2500 to 4000 while $\mathrm{Re}_i=-\mathrm{Re}_o$ is maintained. The radius ratio

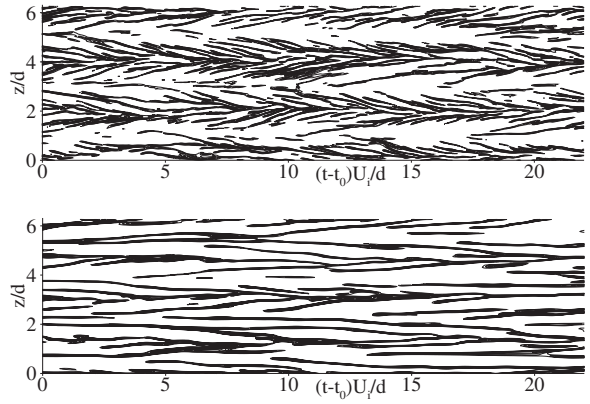

FIG. 1. Herringbone streaks demonstrated by spatial-temporal contours of azimuthal velocity along a line parallel to the z axis and fixed near the inner cylinder wall: (a) Taylor-Couette flow at $\mathrm{Re}=5000$. (b) Counter-rotating Taylor-Couette flow at $\mathrm{Re}_i=-\mathrm{Re}_o=2500$. t_0 is an arbitrary time instant.

is fixed at $\eta=0.5$ for both TC and CRTC flows. The axial dimension of the domain is chosen to be $L_z/d=2\pi$, and 256 Fourier planes are employed in that direction based on the test results in [17]. We have employed 400 spectral elements in the x-y planes, with an element order 8 or 9 in each element.

We begin with a demonstration of the herringbone streaks near the wall. Figure 1(a) shows spatial-temporal contours (z-t plane) of the azimuthal velocity along a line parallel to the z-axis and adjacent to the inner cylinder wall for the TC flow at Re=5000. Shown are eight contour levels between $0.65U_i$ and $0.95U_i$. The distribution reveals fine high-speed streaks tilting alternately at an angle in neighboring cells, reminiscent of the flow photographs of Barcilon *et al.* [11]. In Fig. 1(b) we plot spatial-temporal contours of the azimuthal velocity for the CRTC flow at Reynolds numbers $\mathrm{Re}_i=-\mathrm{Re}_o=2500$. This is similarly based on data along a line oriented in the z direction and adjacent to the inner cylinder, and eight contour levels are shown between $0.57U_i$ and $0.77U_i$. Key characteristics of the streaks observed in the TC flow, such as the herringbone patterns, can also be observed here in the CRTC flow.

Herringbone streaks in TC and CRTC flows share certain common characteristics. For example, they become more populous and tend to be less coherent (persisting shorter in time) with increasing Reynolds number. Comparison of herringbone streaks of TC and CRTC flows at identical Reynolds numbers, $\mathrm{Re}=\mathrm{Re}_i-\mathrm{Re}_o$, shows that the streaks in the latter tend to be less populous and more coherent (persisting longer in time). We note that the visualization of Barcilon *et al.* [11] was conducted with the inner cylinder rotating and the outer cylinder fixed. The present simulations not only confirm the near-wall herringbone streaks in this configuration, but also reveal the presence of such streaks in an additional class of configurations of the counter-rotating Taylor-Couette flow.

We next look into the orientation and the axial distribution of the herringbone streaks. In Figure 2(a) we show a snapshot of the streaks on the inner wall by plotting contours of the instantaneous azimuthal velocity on a grid surface (nearly cylindrical) adjacent to the inner cylinder for the TC flow at Re=5000. Bright and dark regions represent high and low azimuthal velocities, respectively. Evidently the high-speed streaks form herringbonelike patterns, which are clustered around three axial locations for this particular configuration (axial dimension and Reynolds number). Note that the z axis points upward in all plots of Fig. 2, and that the inner cylinder rotates counterclockwise. The orientation of the herringbone patterns apparently resembles the symbols "$\ll$" on the inner cylinder wall.

It has been shown in [17] that although the organized patterns of Taylor vortices can hardly be discerned from the instantaneous velocity field at high Reynolds numbers, they are clearly revealed to underlie the Taylor-Couette turbulence by the time-averaged mean field. To determine the axial locations of the streak clusters relative to the underlying Taylor vortices, we plot in Fig. 2(b) the time-averaged mean field (in a radial-axial plane) of the TC flow at Re=5000. Organized Taylor vortices with scales commensurate to the gap width can be clearly observed. The inflow boundaries (flow from outer wall to inner wall) between Taylor vortices are marked by "I" in the plot, and the outflow boundaries (flow from inner wall to outer wall) are marked by "O." Comparison of Figs. 2(a) and 2(b) shows that the axial loci of inner-wall streak clusters correspond to the outflow boundaries. This indicates that the herringbone streaks concentrate on the outflow boundaries of Taylor vortices on the inner cylinder.

In Fig. 2(c) we show a snapshot of the streaks on the outer wall [same time instant as Fig. 2(a)] by plotting contours of the instantaneous azimuthal velocity on a grid surface (nearly cylindrical) near the outer cylinder. Bright and dark regions again represent high- and low-speed flows, respectively. The streaks (low-speed) on the outer wall are significantly fewer than the streaks (high-speed) on the inner wall, consistent with the observation that turbulent intensity is stronger near the inner wall than near the outer wall in TC flow [17]. However, they appear to similarly form herringbonelike patterns. The sense of tilting, on the other hand, is opposite to that on the inner wall; their orientation resembles the symbols "$\gg$." The streaks are apparently clustered around several axial locations. Comparison between Figs. 2(b) and 2(c) indicates that these locations correspond to the inflow boundaries of the underlying Taylor vortices. Therefore the herringbone streaks on the outer wall concentrate on the inflow boundaries of Taylor vortices, unlike those on the inner cylinder.

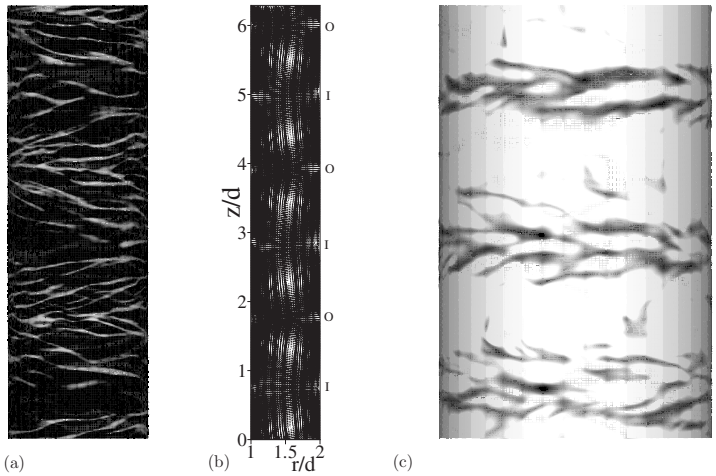

FIG. 2. Orientations and axial loci of herringbone streaks (TC flow, Re=5000): (a) Snapshot of high-speed streaks on a grid surface adjacent to the inner wall; (b) time-averaged mean velocity field in a radial-axial plane (inner wall: $r/d=1$, outer wall: $r/d=2$); and (c) snapshot of low-speed streaks on a grid surface adjacent to the outer wall. Shown in (a) and (c) are contours of the azimuthal velocity. Symbols "O" and "I" represent the outflow and inflow boundaries of Taylor vortex cells.

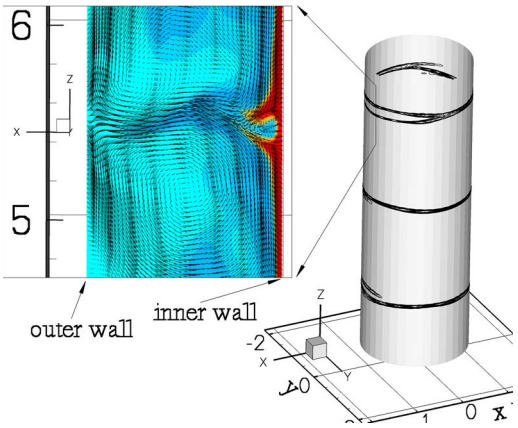

FIG. 3. (Color online) Onset of herringbone streaks: A snapshot of the streaks (contours of azimuthal velocity) on the inner cylinder (TC flow, Re=2000). The inset shows velocity field and azimuthal velocity contours (red or dark color: high velocity; cyan or light color: low velocity) in a radial-axial plane that intersects the forked section of the uppermost streak of the inner wall.

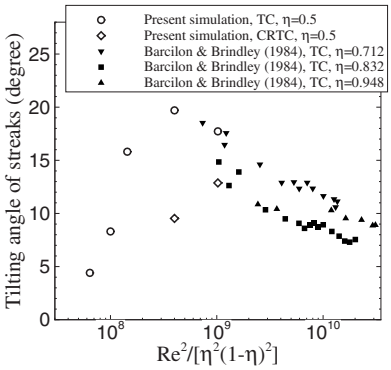

FIG. 4. Average tilting angle of herringbone streaks from present simulations (TC flow and CRTC flow) and Barcilon and Brindley [14] (TC flow).

Herringbone streaks are observed only at sufficiently high Reynolds numbers. As the Reynolds number decreases these streaks will eventually vanish from the wall. To understand their onset we have conducted simulations of the TC flow at a series of Reynolds numbers between Re=1000 and 2500, with an increment ΔRe=500. No herringbone streaks are observed at Re=1500 or below; they can be observed at Re=2000 and above. Figure 3 shows contours of the azimuthal velocity on a grid surface near the inner cylinder for Re=2000, at which the herringbone streaks start to appear (as Reynolds number increases). We can observe streaks engirdling the inner cylinder at three axial locations. One can also observe that they branch at certain sections. For example, the topmost streak forks into two at a section in the plot. In the inset of Fig. 3 we plot the instantaneous velocity field, together with the azimuthal velocity contours in a radial-axial plane that intersects the branching section of the topmost streak. First note the correlation of the presence of streaks with the outflow boundary jet induced by the large-scale Taylor vortices. The jet pumps the high-speed fluid away from the inner wall. This produces a high-speed fluid sheet in the outflow boundary between Taylor vortex cells, which is responsible for the observed high-speed streak on the inner wall. We further observe that a pair of small-scale vortices with the opposite sense of rotation (with respect to the Taylor vortex pair) forms at the outflow boundary toward the inner wall, which apparently splits the high-speed fluid sheet and thus results in the forked streak on the wall. By examining the flow fields in different radial-axial planes, we observe that this small vortex pair persists only on a section of the cylinder circumference and extends away from the wall along the azimuthal direction. The branching point in the topmost streak corresponds to where this small vortex pair originates.

The large-scale Taylor vortices (with scales commensurate to the cylinder gap) appear to play a significant role. At Reynolds numbers below the onset of herringbone streaks, the outflow boundary jet induced by the Taylor vortices facilitates the formation of streaks (which do not branch or appear like herringbone yet) by pumping the high-speed fluid away from the inner wall. At the onset, the streaks branch due to the formation of near-wall small-scale vortices at the outflow boundaries. The branching multiplies as the Reynolds number increases, and the streaks eventually attain the herringbonelike appearance. This suggests that the outflow boundary of Taylor vortices is the precursor to the herringbone streaks on the inner wall, and that the formation of near-wall small-scale vortices is intimately related to the proliferation of these streaks. Similar observations can be made for the streaks on the outer wall.

We next investigate the Reynolds number dependence of the tilting angle of herringbone streaks. Barcilon and Brindley [14] showed tilting angle data (TC flow) for a range of very high Reynolds numbers (roughly Re=10 000–200 000) obtained from flow visualizations. The trend of their data suggests that within that range the tilting angle increases as the Reynolds number decreases. This trend may not sustain as the Reynolds number further decreases, however, because at sufficiently low Reynolds numbers the herringbone streaks will disappear (e.g., no herringbone streaks at Re=1500 and below for radius ratio η=0.5). There may be two possibilities as the Reynolds number further decreases (when the streaks are about to disappear): the tilting angle decreases or the streaks maintain a high tilting angle but decrease in amplitude (or length).

To investigate the tilting angle variation and the above possibilities, we have computed the tilting angles of herringbone streaks at the Reynolds numbers that have been simulated for the TC flow and the CRTC flow. The tilting angle can be determined from the spatial-temporal velocity data employing the Taylor hypothesis [17]. In Fig. 4 we plot the average magnitude of the tilting angle as a function of a characteristic Reynolds number, $\mathrm{Re}^2/[\eta^2(1-\eta)^2]$, as prescribed by Barcilon and Brindley [14]. We have included results from present simulations for the TC flow and CRTC flow (η=0.5), together with the data from Barcilon and Brindley for the TC flow at three other radius ratios. When plotting the data points of the CRTC flow we have used the Reynolds number defined by $\mathrm{Re}=\mathrm{Re}_i-\mathrm{Re}_o$. One can first observe that the tilting angles of the herringbone streaks in the

CRTC flow are notably lower than those in the TC flow at identical Reynolds numbers ($\mathrm{Re}=\mathrm{Re}_i-\mathrm{Re}_o$). For the TC flow, the data from present simulations extends the range of $\mathrm{Re}^2/[\eta^2(1-\eta)^2]$ to much lower values with respect to Barcilon and Brindley's data. In the range where the two data sets overlap, the tilting angle values from both sets are in good agreement. The composite of the present simulation data and Barcilon and Brindley's data provides a comprehensive picture about the variation of the tilting angle over a wide range of Reynolds numbers in the TC flow: At very low Reynolds numbers no herringbone streaks exist on the wall; after the herringbone streaks emerge, with increasing Reynolds number the tilting angle first increases, reaching a peak value at some point, and then decreases as the Reynolds number further increases. In addition, the simulation data indicates that as the Reynolds number decreases and the herringbone streaks are about to disappear while their tilting angle approaches zero their amplitudes (length) do not go to zero but rather stay of order one.

Nearly three decades ago Barcilon *et al.* [11] revealed the presence of a fine pattern of streaks on the cylinder wall at high Reynolds numbers. They described this organized pattern as "herringbone" because of its appearance. These herringbone streaks have remained a mystery since then, and little is known about their characteristics. In this Rapid Communication we have characterized several aspects of the herringbone streaks employing three-dimensional direct numerical simulations. We have shown that these streaks exist not only in Taylor-Couette turbulence but also in counterrotating Taylor-Couette turbulence. The herringbone patterns have opposite senses of tilting on the inner and outer cylinder walls. While they concentrate on the outflow boundaries of Taylor vortices on the inner wall, on the outer wall they concentrate on the inflow boundaries. We have also demonstrated that the tilting angle of the streaks has a peak value corresponding to a certain Reynolds number, and that it decreases toward both very low and very high Reynolds numbers.

The author gratefully acknowledges the support of the NSF. Computer time was provided by the TeraGrid and the Rosen Center for Advanced Computing at Purdue University.

[1] M. Couette, Ann. Chim. Phys. **21**, 433 (1890).
[2] G. Taylor, Philos. Trans. R. Soc. London, Ser. A **223**, 289 (1923).
[3] D. Coles, J. Fluid Mech. **21**, 385 (1965).
[4] K. T. Coughlin, P. S. Marcus, R. P. Tagg, and H. L. Swinney, Phys. Rev. Lett. **66**, 1161 (1991).
[5] D. P. Lathrop, J. Fineberg, and H. L. Swinney, Phys. Rev. Lett. **68**, 1515 (1992).
[6] A. Prigent, G. Gregoire, H. Chate, O. Dauchot, and W. van Saarloos, Phys. Rev. Lett. **89**, 014501 (2002).
[7] C. Andereck, S. Liu, and H. Swinney, J. Fluid Mech. **164**, 155 (1986).
[8] J. J. Hegseth, C. D. Andereck, F. Hayot, and Y. Pomeau, Phys. Rev. Lett. **62**, 257 (1989).
[9] K. Coughlin and P. S. Marcus, Phys. Rev. Lett. **77**, 2214 (1996).
[10] P. W. Colovas and C. D. Andereck, Phys. Rev. E **55**, 2736 (1997).
[11] A. Barcilon, J. Brindley, M. Lessen, and F. Mobbs, J. Fluid Mech. **94**, 453 (1979).
[12] S. Kline, W. Reynolds, F. Schraub, and P. Runstadler, J. Fluid Mech. **30**, 741 (1967).
[13] C. Smith and S. Metzler, J. Fluid Mech. **129**, 27 (1983).
[14] A. Barcilon and J. Brindley, J. Fluid Mech. **143**, 429 (1984).
[15] H. Görtler, NACA Technical Memorandum 1375 (1954).
[16] T. Wei, E. Kline, S. Lee, and S. Woodruff, J. Fluid Mech. **245**, 47 (1992).
[17] S. Dong, J. Fluid Mech. **587**, 373 (2007).
[18] S. Dong, G. Karniadakis, A. Ekmekci, and D. Rockwell, J. Fluid Mech. **569**, 185 (2006).